



Evolution of soil erosion rates in alpine soils of the Central Rocky Mountains using fallout Pu and $\delta^{13}\text{C}$

Raquel Portes^{a,*}, Dennis Dahms^b, Dagmar Brandová^a, Gerald Raab^a, Marcus Christl^c, Peter Kühn^d, Michael Ketterer^e, Markus Egli^a

^a Department of Geography, University of Zurich, Winterthurerstrasse 190, CH-8057 Zurich, Switzerland

^b Department of Geography, University of Northern Iowa, Cedar Falls, IA 50614-0406, USA

^c Laboratory of Ion Beam Physics, ETH Zurich, 8093 Zurich, Switzerland

^d Research Area Geography, Soil Science and Geomorphology, Department of Geosciences, University of Tübingen, Rümelinstrasse, 19-23, 72070 Tübingen, Germany

^e Chemistry Department, Metropolitan State University of Denver, Campus Box 52, Denver, CO 80217-3362, USA

ARTICLE INFO

Article history:

Received 27 October 2017

Received in revised form 29 May 2018

Accepted 3 June 2018

Available online 19 June 2018

Editor: M. Frank

Keywords:

slope stability

Pu isotopes

carbon isotopes

soil chronosequence

Late Pleistocene

Wind River Range

ABSTRACT

Data from soil chronosequences have been widely used to quantify soil formation and weathering rates, but are less used to determine erosion rates and the stabilisation of moraines over time. We hypothesise that soil erosion rates on moraine hillslopes decrease over time as soils evolve and slopes stabilise. We selected a sequence of moraines in the Wind River Range (Central Rocky Mountains) to study these processes over time. Moraine ages were based on ^{10}Be surface exposure dating of moraine boulders. Quantitative soil erosion and accumulation rates along slopes with similar exposures, lengths and gradients were determined from profile patterns of $^{239+240}\text{Pu}$ radionuclides. We used stable carbon isotopes ($\delta^{13}\text{C}$) in relation with the total soil organic carbon (SOC) content for qualitative information about soil erosion. The ^{10}Be boulder exposure ages revealed that the moraines were deposited during the Younger Dryas and the pre Bølling–Allerød episodes of the late Pleistocene. The morphology of the soils suggests a complex history of development and shows that both erosion and aeolian deposition have affected the soils. The $^{239+240}\text{Pu}$ measurements revealed that erosion rates strongly decrease with time as soils develop. A weakly developed soil (Cambisol) is found on the youngest moraine (11.8 ka) that exhibits an erosion rate, depending on the calculation procedure, in the range of 260 to 520 $\text{t km}^{-2} \text{a}^{-1}$. With time the erosion rate rapidly decreases to almost zero, presumably as a full vegetation cover develops. Bioturbation and/or dust influx is increasingly obvious with increasing age of the soils, as evidenced by the comparison of $\delta^{13}\text{C}$ and SOC. The mass balance of the oldest soil (15.8 ka) indicates that the slopes have reached a geomorphological stability with little or no net erosion. Aeolian influx appears to be the primary factor to account for mass changes in the oldest soil.

© 2018 Elsevier B.V. All rights reserved.

1. Introduction

To date, most studies evaluating rates of soil erosion have focused on the impact of soil tillage on agricultural lands (Quine and Walling, 1991) and on the comparison between cultivated and uncultivated soils (He and Walling, 1997; Lal et al., 2013; Zhang et al., 1990), while few have focused on natural environments, such as forested slopes (Meusburger et al., 2013) or high alpine areas (Zollinger et al., 2015). We know of no studies, to

date, that concern how rates of erosion (or accumulation) evolve as a function of time and soil development.

Besides slope gradient and soil cover, soil erodibility is strongly linked to soil characteristics such as particle size distribution, stoniness, structure, permeability, water content and organic matter content (Wischmeier and Smith, 1960; Lal and Elliot, 1994). Numerous studies demonstrate that these soil characteristics change over time as soils evolve (Dahms et al., 2012). Soil chronosequences are a powerful tool widely used on moraine sequences to examine soil development over time. Because they enable us to estimate rates of soil formation (Bockheim, 1980; Huggett, 1998; Dahms et al., 2012) this approach also can be useful to evaluate the evolution of soil erosion rates over time. Soils of different ages may therefore give valuable insight into the tem-

* Corresponding author.

E-mail address: raquel.decastroportes@geo.uzh.ch (R. Portes).

poral evolution of soil erosion. When suitable sites are available, radionuclides have been shown to be reliable tracers for estimates of soil erosion.

Fallout radionuclides (FRNs) (e.g. ^{137}Cs and $^{239+240}\text{Pu}$) have been widely used to trace mid-term (decadal) soil erosion (or accumulation) rates in natural and agricultural areas worldwide (Alewell et al., 2014; He and Walling, 1997). FRNs were mainly emitted to the upper atmosphere by above-ground nuclear weapons testing during the 1950–1960's and/or by nuclear reactor accidents (e.g. Chernobyl 1986). When deposited on the soil surface, they strongly bond to solid phases due to their high ionic potential, which makes them insoluble. Therefore, their removal from soil can be associated with soil erosion processes more directly than chemical (leaching), translocation or biological processes (Ketterer et al., 2011). FRNs inventories provide information of soil mass movement per unit area only over the past 50–60 yrs (Alewell et al., 2014; Lal and Elliot, 1994). The rates are estimated by comparing tracer inventory at various soil depths to a nearby non-eroding reference site. The reference site is assumed to have negligible soil erosion or deposition, thus each site represents the total tracer inventory (He and Walling, 1996). The tracer inventory in non-eroding sites is lost by radioactive decay, while erosional sites lose tracer by both decay and erosion (Lal et al., 2013). The correlation of stable carbon isotopes signatures (i.e. $\delta^{13}\text{C}$) and soil organic carbon content can qualitatively indicate long-term disturbances in aerated soils, where high correlations reflects the enrichment of ^{13}C in depth as soil organic carbon decomposes in non-eroded soils (Alewell and Schaub, 2009; Meusburger et al., 2013; Zollinger et al., 2015). Due to isotopic fractionation during plant decomposition, residues are increasingly enriched in the heavier carbon isotope (^{13}C) as the lighter ^{12}C will preferentially be involved in biochemical reactions (Alewell and Schaub, 2009). In undisturbed soils, therefore, increasing $\delta^{13}\text{C}$ values and decreasing total org. C contents with depth would be typical and should correlate with the pattern of erosion rates determined by the Pu-isotopes.

In this study, we test the hypothesis that soil erosion rates on moraine hillslopes decrease over time as soils evolve. To test this hypothesis, we chose a location in the Wind River Range (WRR; Central Rocky Mountains) with a previously-described and mapped sequence of moraines and slopes related to post-LGM (Last Glacial Maximum; post-Pinedale) glacial activity (Dahms et al., 2010). Hence, our objective is to quantitatively assess soil erosion or accumulation rates using a chronosequence approach combined with fallout radionuclides ($^{239+240}\text{Pu}$). In addition, we expected that $\delta^{13}\text{C}$ and organic C in the soils correlate most strongly with increasing age of the soils and decreasing rates of erosion. Erosion rates were – with purpose – not investigated using cosmogenic nuclides (such as ^{10}Be and others). These isotopes only give an average value over the entire period of pedogenesis. To better trace the evolution of soil erosion, moraine slopes having a different age should be investigated by using isotopes that give a more instantaneous signal. FRNs are ideal tracers for this purpose and reflect the actual state (i.e. last few decades). Using this approach, we should be able to quantify soil erosion over time on moraine slopes in an alpine area and to approximate the age(s) during which these moraines are stabilised and erosional losses minimised.

2. Study area

The Wind River Range (WRR) is located in the central Rocky Mountains of west-central Wyoming, USA (Fig. 1a). The range trends Northwest–Southeast with a length of approximately 225 km and a width of 48 km (Fig. 1b; Dahms, 2002; Keefer, 1970). The lithology of the range is mainly composed of early Precambrian granitoid batholith (Keefer, 1970). Sedimentary rocks with

different ages and compositions surround the batholith's range: Eocene sandstones and shales bound the west flank while Paleozoic and Mesozoic limestones, siltstones and sandstones form hogback ridges along the eastern flank of the range (Keefer, 1970). The WRR belongs entirely to the Greater Yellowstone Ecosystem and its major part to the Bridger-Teton and Shoshone national forests and wilderness areas. Vegetation is characterised by alpine tundra above ~ 3200 m and conifer forest below (Dahms et al., 2010). In the Cirque of the Towers (Fig. 1b, c; located in the southern WRR), mean annual precipitation varies around 1100 mm/yr and mean annual temperature is about -3.7°C (Dahms, 2002).

First investigations of allostratigraphic units in the WRR (alpine to high alpine areas; from the northern to the southern parts of the WRR) and soils were reported by Dahms et al. (2010). In general, the soils are rather shallow but enable a distinction of younger from older moraine deposits. The soils vary from Lithosols (youngest soils) to Luvisol or Cambisols with transition to Podzols (oldest soils). Two types of B horizons were recognised; those based mainly on colour are Bw horizons, whereas those based on both colour and an increase in clay content are Bt horizons (Dahms et al., 2010). Typically, many soils exhibit a thin loess mantle that has been deposited since the end of the last glaciation. Several studies have demonstrated that much of the silt and clay in soils developed on alpine moraines in the WRR has an atmospheric origin, which is evidenced by aeolian signals in the particle size distribution, heavy mineral fractions and geochemical signatures (Applegarth and Dahms, 2004; Dahms and Rawlins, 1996).

Due to the relatively dry environmental conditions, dust input is not only related to glacial periods; there also is evidence for modern-day aeolian inputs to soils of the WRR (Applegarth and Dahms, 2004; Dahms and Rawlins, 1996). Dust particles are those that have been entrained by the wind and transported without contact with the ground surface. This distinguishes dust particles (mainly coarse-to-medium silt) from larger grains, such as sand, that can also be transported by the wind. Sand-sized particles, when transported by the wind, do so largely by saltation, a bouncing type of particle motion with periodic contact with the ground surface, or by surface creep, where there is constant contact with the ground surface during horizontal transport (Muhs, 2013). Loess is recognised in the field by its silt loam texture which contrasts markedly with the underlying gritty sandy loam or loamy sand matrix (Shroba and Birkeland, 1983). Horizons with some loess can be loamy when silt loam loess is mixed with coarser materials.

3. Materials and methods

3.1. Experimental set-up and soil sampling

The Cirque of the Towers (Fig. 1b, c) was chosen as study site because of its well-mapped sequence of moraines related to post-LGM (post-Pinedale) glacial activity (Dahms et al., 2010). Based on Dahms et al.'s (2010) map of this cirque, we selected a sequence of three moraines with different, relative age estimates. To better constrain our age constraints, the moraines were dated using surface exposure dating (^{10}Be) of moraine boulders. The moraines were selected based on published maps of the WRR showing the late Quaternary glacial and periglacial deposits (Dahms et al., 2010). These authors correlated the allostratigraphic units and assigned them to the Holocene (e.g. Alice Lake alloformation) and Pleistocene (e.g. Temple Lake alloformation). No numeric ages were presented. We sampled moraine boulders for surface exposure dating (^{10}Be) according to the sampling guidelines of Gosse and Phillips (2001). We chose large, flat-topped boulders to avoid edge effects protruding more than 2 m from the surrounding sediments (Masarik and Wieler, 2003). The position (latitude/longitude and altitude)

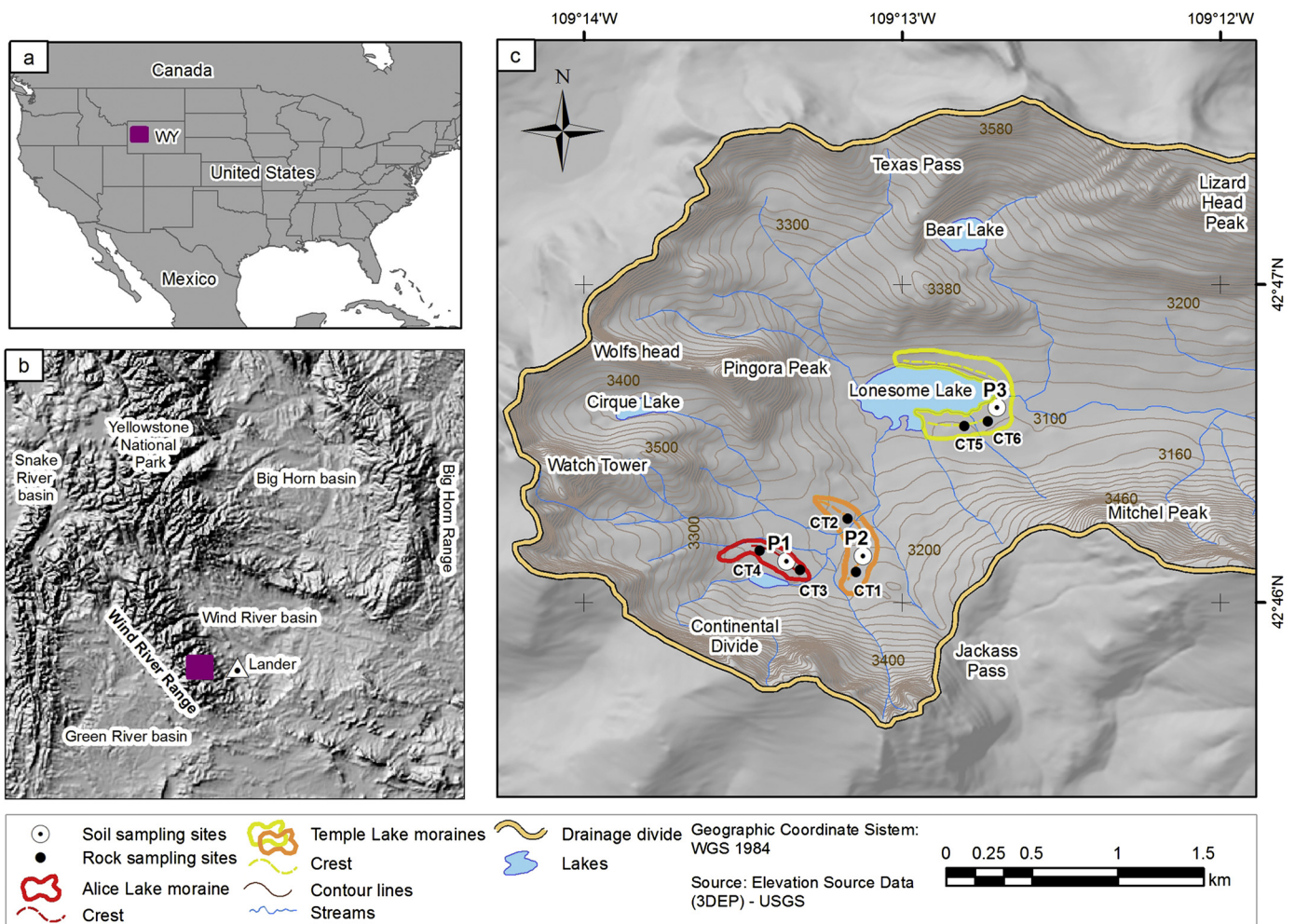


Fig. 1. a) Location of the Wind River Range (pink square) within North America. b) Regional location map of the Wind River Range. The pink square represents the location of the Cirque of the Towers. c) Detailed location map of the Cirque of the Towers showing the sampling sites. P1–P3: investigated pedons. Close nearby to these pedons are the reference and erosion sites for Pu and $\delta^{13}\text{C}$ measurements (Table 1); CT1–CT6: sampled boulders (for ^{10}Be dating). (For interpretation of the colours in the figure(s), the reader is referred to the web version of this article.)

of the sample sites was recorded with GPS and verified with topographic maps. The geometry of each boulder and the effect of topographic shielding by surrounding mountains were assessed. Because cosmic rays are distinctly attenuated within the rock material, production of cosmogenic isotopes is highest at the surface; thus, we sampled the uppermost 1–3 cm of the rock surface and documented the sample thickness.

On each of the three moraines (Alice Lake, Temple Lake and Lonesome Lake), we proceeded as follows:

i) We sampled one soil profile at the crest (Fig. 1c; Table 1). Soil pits were excavated to the C horizon where possible. Soil descriptions were carried out according to FAO guidelines (FAO, 2006) and the soils classified according to IUSS Working Group WRB (2014). Vegetation cover was estimated at each site on the basis of visual estimation in the field (in % cover; ocular estimation of the cover; done as ‘canopy’ cover; Whittaker, 1962). Root abundance and size in the profiles were assessed following FAO (2006).

ii) For the determination of soil erosion and accumulation rates using $^{239+240}\text{Pu}$ and $\delta^{13}\text{C}$, we sampled on each moraine:

- ‘Reference’ profiles (0–20 cm; using a soil corer) at undisturbed flat locations on each moraine where erosion and accumulation processes could reasonably be assumed to be negligible for the last 50 to 60 yrs (that corresponds to the time range covered by Pu-isotopes).

- ‘Erosion sites’ (0–20 cm; using a soil corer) that were located on the backslope of the moraines with north to northeast aspects, slope inclinations of 25% and lengths of 15–21 m (Table 1). Erosion or accumulation rates were always calculated in comparison to the corresponding reference site.
- We took four replicate profiles at each of the reference and erosion sites. Soil samples for $^{239+240}\text{Pu}$, $\delta^{13}\text{C}$ and org. C analyses were taken from the soil corer at 5 cm increments from 0–20 cm depths. The soil cores were also used to determine bulk densities.

3.2. Soil analyses

Samples were oven-dried at 70 °C and sieved (<2 mm) prior to analysis. Prior to grain size analysis, 60 g of fine earth were dispersed in a 3% H_2O_2 solution to digest soil organic matter. The grain size distribution was determined by combination of wet-sieving of the coarser particles (2000–32 μm) and X-ray granulometry (SediGraph 5100) measurements for the finer particles (32–1 μm). Soil pH was determined using a soil:solution (0.01 M CaCl_2) ratio of 1:2.5.

The $\delta^{13}\text{C}$ signature tends to become less negative with soil depth due to the relative increase in the heavier ^{13}C (Alewell and Schaub, 2009). We expected that the change in $\delta^{13}\text{C}$ content with soil depth would parallel the decrease in carbon content.

Table 1
Characteristics of the investigated sites of the Cirque of Tower, Wind River Range.

Site	Assumed age of the moraine (Dahms et al., 2010)	Pedon	Site type	Elevation (m a.s.l.)	Latitude/Longitude (°N/°E)	Landform	Aspect (°N)	Slope (%)	Slope position	Slope form	Slope length (m)	Parent material	Vegetation	Vegetation cover (%)
Alice Lake	Holocene	P1	Reference	3213	42.7687/−109.2229	End moraine	60	1	Crest	Flat	–	Granitic till	Alpine tundra	50
			Erosion	3210	42.7687/−109.2229	End moraine	60	25	Backslope	Straight	–	Granitic till	Alpine tundra	50
Temple Lake	Pleistocene	P2	Reference	3190	42.7683/−109.2182	Lateral moraine	350	3	Crest	Flat/slightly concave	–	Granitic till	Alpine tundra/Krummholz	72
			Erosion	3193	42.7683/−109.2182	Lateral moraine	350	27	Backslope	Straight	–	Granitic till	Alpine tundra/Krummholz	72
Lonesome Lake	older than Temple lake	P3	Reference	3104	42.7770/−109.2130	End moraine	45	1	Crest	Flat	–	Granitic till	Montane forest	97
			Erosion	3100	42.7770/−109.2130	End moraine	45	27	Backslope	Straight	–	Granitic till	Montane forest	97

Soil erosion processes have been shown to weaken this correlation (Alewell and Schaub, 2009; Zollinger et al., 2015). The $\delta^{13}\text{C}$ isotopic ratios were measured using a Picarro analyser (G2131-i Picarro) for isotopic CO_2 (Combustion Module-Cavity Ring Down Spectroscopy (CM-CRDS), Sunnyvale, California, USA). Instrumental measurement uncertainty is 0.1%. Soil powder (milled fine earth) was weighed into tin capsules and combusted at 950 °C. The released CO_2 was measured using a CRDS analyser (Picarro, G2131 type). We used an internal standard (30B00GW9 Chernozem 2013) for every 6 samples in order to correct for potential drift in the $\delta^{13}\text{C}$ and C content values.

We used the rock fragments and several fractions of the fine earth as diagnostic criteria for the identification of any lithological discontinuities in the profile (Schaeztl, 1998; FAO, 2006).

3.3. Sample preparation and measurement for ^{10}Be surface exposure dating

Cosmogenic nuclides can be used for both surface age determination and calculation of erosion or denudation rates (Balco et al., 2008). In our case, we used ^{10}Be for deriving age constraints of the investigated moraines. We obtained numeric age-estimates for the moraines from ^{10}Be surface exposure dating of two large granitic boulders (>2 m in height) on each moraine. The rock samples were pre-treated following the procedures according to Kohl and Nishiizumi (1992). Samples were crushed and sieved and the quartz isolated by treating the 0.25–0.6 mm fraction with *aqua regia* to destroy organic contaminations and any calcareous components. After a 1 h-treatment with 0.4% HF, we used a floatation system to physically separate feldspar and mica components from quartz. Remaining non-quartz remnants were removed by repeated leaching by 4% HF. Once pure quartz was obtained, we added a ^9Be -carrier solution and dissolved the samples in 40% HF. Be was isolated using anion and cation exchange columns followed by selective pH precipitation techniques (von Blanckenburg et al., 1996). The Be hydroxides then were precipitated, dried, and calcinated to BeO at 850 °C. $^{10}\text{Be}/^9\text{Be}$ ratios were measured at the ETH Laboratory of Ion Beam Physics' Accelerator Mass Spectrometry (AMS) facility using the ^{10}Be standard S2007N with a nominal value of $^{10}\text{Be}/^9\text{Be} = 28.1 \times 10^{-12}$ (Christl et al., 2013). S2007N has been calibrated to the ^{10}Be standard ICN 01-5-1 of Nishiizumi et al. (2007) and has a nominal $^{10}\text{Be}/^9\text{Be}$ value of 2.709×10^{-11} . The 1σ error of S2007N is 2.7% (Christl et al., 2013). Measured $^{10}\text{Be}/^9\text{Be}$ ratios were corrected for ^{10}Be contributed by the Be-carrier (blank value: 0.003E-12). ^{10}Be concentrations and according one sigma uncertainties are reported in Table 2. ^{10}Be exposure ages were calculated using CRONUS-Earth (<http://hess.ess.washington.edu/math/>) version 2.3 with a ^{10}Be half-life of 1.387 ± 0.012 Ma (Chmeleff et al., 2010). The production rate was corrected for latitude and altitude using the scaling scheme of Stone (Stone, 2000) and corrected for sample thickness assuming an exponential depth profile with an effective radiation attenuation length of 160 g cm^{-2} (Gosse and Phillips, 2001) and a rock density of 2.7 g cm^{-3} . Effects of variations of the geomagnetic field on the ^{10}Be age are said to be negligible (Pigati and Lifton, 2004).

3.4. Sample preparation and measurement for $^{239+240}\text{Pu}$ activities

Sample preparation was done according to Ketterer et al. (2004). The samples obtained from the soil cores (erosional and reference sites) were analysed for $^{239+240}\text{Pu}$. Five grams of the milled fine earth ($\approx 60 \mu\text{m}$) was dry-ashed for 20 h at 600 °C to remove organic matter. A spike of ca. 30 picograms (0.0044 Bq) of ^{242}Pu tracer solution (NIST 4334) was added to the sample vials. The samples were then leached using 10 mL of 16 M HNO_3 in

Table 2¹⁰Be measurements of the moraine boulders of the Cirque of Towers, Wind River Range.

Site	Sample name	Latitude (°N)	Longitude (°W)	Elevation (m a.s.l.)	Sample thickness (cm)	Shielding correction	¹⁰ Be ^{a,b} (10 ⁵ atoms g ⁻¹ qtz)	¹⁰ Be surface exposure age ^{c,d,e} (a)
Alice Lake (P1)	CT3	42.76873	-109.2229	3225	1.8	0.930	4.4 ± 0.14	11285 ± 1030 (358)
Alice Lake (P1)	CT4	42.76873	-109.2229	3225	3.0	0.935	4.8 ± 0.19	12406 ± 1174 (499)
Temple Lake (P2)	CT1	42.76833	-109.2182	3216	2.5	0.947	6.2 ± 0.18	15937 ± 1442 (462)
Temple Lake (P2)	CT2	42.76828	-109.2176	3214	3.2	0.954	5.9 ± 0.20	15162 ± 1395 (507)
Lonesome Lake (P3)	CT5	42.72660	-109.2111	3125	3.0	0.972	5.7 ± 0.18	15253 ± 1390 (472)
Lonesome Lake (P3)	CT6	42.72660	-109.2111	3125	2.2	0.972	6.1 ± 0.19	16267 ± 1483 (504)

^a We used a density of 2.7 g cm⁻³ for all samples.^b Uncertainty includes AMS measurements errors and statistical counting error.^c External (internal) uncertainty.^d We used zero rock erosion rates for all samples.^e Surface exposure ages were calculated with the CRONUS-Earth online calculators (<http://hess.ess.washington.edu/>, Balco et al., 2008 and version 2.3) and using scaling scheme for spallation based on Stone (2000).

a heating oven at 75 °C for 20 h. After acid leaching, the samples were filtered into a 50 mL centrifuge tube and adjusted to a concentration of 8 M HNO₃. Pu species were adjusted to a Pu⁴⁺ oxidation state using an acidified FeSO₄·7H₂O solution (2 mg/mL of leached solution) and NaNO₂ solution (20 mg/mL of solution). The Fe²⁺ solution was added first and subsequently the sodium nitrite solution. Thereafter, the samples were heated at 75 °C for 2 h. After the oxidation process, TEVA resin (Triskem-international 100–150 μm; 2 mg of TEVA per mL of leached solution) was added to the centrifuge tubes and shaken using a horizontal shaker for 2 h so that the TEVA uptakes the tetravalent Pu. Thereafter the resin was collected using a pipet tip containing glass wool plug. The pipet tips were rinsed to remove tetravalent actinides (i.e. U and Th) using acid solutions in the following order: 5 × 2 M HNO₃; 3 × 8 M HCl; 2 × 2 M HNO₃ (rinse volume: 1 ml per 30 mg of TEVA). Pu was eluted into Eppendorf tubes using 0.4 ml 0.05 M ammonium oxalate and diluted with water to a 1.2 ml final volume. Each batch contained 37 samples and 13 controls: 3 pre-bomb soils as a ‘negative control’, 2 Standard Reference Material 4350 b (river sediment for radioactivity measurements from NIST), 3 blanks and 5 duplicates of soil samples.

The measurements of Pu isotopes were carried out using an Agilent 8800 Triple Quadrupole ICP-MS. The ICP-MS instrument was equipped with a high-efficiency desolvating sample introduction system (APEX HF, ESI Scientific, Omaha, NE, USA). A detection limit of <0.1 Bq/kg ²³⁹⁺²⁴⁰Pu was obtained for samples of nominal 1 g of dry-ashed material; for ²³⁹⁺²⁴⁰Pu activities >1 Bq/kg, the measurement error was 1 to 3%.

3.5. Conversion of ²³⁹⁺²⁴⁰Pu activities into soil erosion and accumulation rates

The inventories (Bq/m²) of ²³⁹⁺²⁴⁰Pu were calculated based on the following equation:

$$A(s) = \frac{1}{S} \sum_i M_{Ti} C_i \quad (1)$$

where C_i is the activity of the i th sub-sample depth increment (Bq/kg); M_{Ti} is the total mass of the i th sample depth increment (kg) and S is the area of the horizontal core cross (m²). Soil erosion or accumulation rates were calculated by comparing the isotope inventory for an eroding site with the corresponding inventory of the reference site where neither erosion nor soil accumulation are assumed.

Then, two different models were used to convert ²³⁹⁺²⁴⁰Pu inventories into soil erosion rates.

1) The profile distribution model (PDM) according to Walling and Quine (1990) and Zhang et al. (1990):

$$A'(x) = A_{ref}(1 - e^{x/h_0}) \quad (2)$$

where $A'(x)$ is the amount of isotope inventory above depth x (Bq/m²), x is the depth from soil surface expressed as mass between top and actual depth (kg/m²), A_{ref} is the reference inventory as mean of all reference sites (Bq/m²) and h_0 is the profile shape factor (kg/m²) that is a coefficient describing the rate of exponential decrease in inventory with depth for soil profiles in uncultivated sites.

The erosion rate Y was calculated according to Walling and He (1999) and Zhang et al. (1990):

$$Y = \frac{10}{t - t_0} \times \ln \left(1 - \frac{X}{100} \right) \times h_0 \quad (3)$$

where Y is erosion rate (t/ha/a), t is the year of sampling (i.e. 2016), t_0 is a reference year (i.e. 1963) for thermonuclear weapon testing commonly used in for ²³⁹⁺²⁴⁰Pu, X is % reduction of total inventory (A_u [Bq/m²]) in relation to the local reference value ($(A_{ref} - A_u)/A_{ref} \times 100$).

2) The inventory method (IM) according to Lal et al. (2013):

$$L = -\frac{1}{\alpha P} \ln \left(1 - \frac{I_{loss}}{I_{ref}} \right) \quad (4)$$

where L is loss of soil, I_{loss} is $I_{ref} - I$, I_{ref} is the local reference inventory as mean of all reference sites (Bq/m²) and P is particle size correction factor, where $P > 1$. Corrections were done using a P factor of 1 and 1.2 according to Walling and He (1999) and 1.5 according to Lal et al. (2013). These factors take into account that erosion processes act in a selective way, removing or depositing fine particles and because of Pu is preferentially adsorbed in such fine particles (He and Walling, 1996), we used these correction factors to avoid overestimation of the soil erosion rates. The coefficient α was obtained from a least squared exponential fit of the ²³⁹⁺²⁴⁰Pu depth profile (Alewell et al., 2014).

4. Results

4.1. ¹⁰Be surface exposure ages

¹⁰Be measurements of the moraine boulders (Table 2) show that the Alice Lake (P1 in Fig. 1c, Table 1) moraine is the youngest, with ages of 11.3 and 12.4 ka (considering the internal errors and error propagation, this gives an average age of 11.8 ± 0.3 ka). Ages of the boulders on the Temple Lake (P2 in Fig. 1c, Table 1) and Lonesome Lake (P3 in Fig. 1c, Table 1) moraines are quite similar. Exposure ages of the Temple Lake moraine boulders are 15.2 and 15.9 ka (average age = 15.5 ± 0.3 ka) and the ages of boulders on the Lonesome Lake moraine are 15.3 and 16.3 ka (average age = 15.8 ± 0.3 ka).

Table 3
Soil physical, chemical and morphological properties of the investigated soils.

Pedon Horizon	Depth (cm)	Munsell colour Moist	Bulk density (g/cm ³)	Soil skeleton (wt%) ¹	TOC ² (g/kg)	pH ³	Soil structure			Consistence		S ⁹	P ¹⁰	Roots	
							Grade ⁴	Type ⁵	Size ⁶	Dry ⁷	Moist ⁸			A ¹¹	S ¹²
P1 Alice Lake – Cambisol (Humic, Loamic)															
A1	0–15	10YR3/1	1.0	4.6	29.2	5	WE	SG	–	LO	VFR	NST	NPL	M	F
2A2	15–28	10YR3/2	1.1	12.2	14	5.4	WM	GR	FI	SO	VFR	NST	NPL	M	F
2Bw	28–43	10YR4/4	1.1	31.9	6.5	5.3	WM	GR	FI	SO	FI	SST	PL	M	F
3Cox/Bw	43–70+	10YR3/4	1.3	38.3	2.5	5.3	WE	GR	FI	SO	VFR	NST	NPL	C	F
P2 Temple Lake – Protostagnic Cambisol (Humic, Loamic, Raptic)															
A	0–17	10YR2/1	0.8	8.4	51.9	4.3	WE	GR	FI	LO	FR	NST	NPL	M	F, M
2Bwg1	17–40	10YR3/3	0.7	3.4	23.3	4.4	WM	GR	FI	SO	FI	SST	PL	M	F, M
3Bwg2	40–78+	10YR3/6	0.9	6.4	21.8	4.7	WE	GR	FI	SO	FR/FI	SST	SPL	M	F, M
P3 Lonesome Lake – Entic Podzol (Arenic)															
O	0–5	10YR2/2	–	6.5	110.4	4.5	WE	SG	–	LO	LO	NST	NPL	M	F, M, C
A	5–17	10YR3/3	0.8	6.5	29.3	4.7	WE	GR	FI	SO	FR	SST	NPL	M	F, M, C
2EB	17–30	10YR3/4	0.9	8.4	21.3	4.9	WE	GR	FI	SHA	FR	SST	NPL	M	F, M, C
3Bs	30–45	7.5YR4/6	1.2	17.6	12	5	WE	GR	FI	SHA	FR	SST	NPL	F	F, M, C
3Cox/B	45–55+	2.5Y4/4	1.7	20.1	3	5.8	WE	GR	FI	LO	LO	NST	NPL	F	F, M, C

¹ Material >2 mm in diameter.

² TOC = Total organic carbon.

³ pH CaCl₂.

⁴ WE = Weak; WM = Weak to moderate.

⁵ SG = Single grain; GR = Granular.

⁶ FI = Fine/thin.

⁷ LO = Loose; SO = Soft; SHA = Slightly hard.

⁸ LO = Loose; VFR = Very friable; FR = Friable; FI = Firm.

⁹ S = Stickiness; NST = Non-sticky; SST = Slightly sticky.

¹⁰ P = Plasticity; NPL = Non-plastic; PL = Plastic.

¹¹ A = Root abundance; F = Few; C = Common; M = Many.

¹² S = Root size; F = Fine; M = Medium; C = Coarse.

Table 4
Particle-size distribution of the investigated soils.

Pedon/ Horizon	Depth	Particle-size distribution ¹																
		Sand (g/kg)	Very coarse sand (g/kg)	Coarse sand (g/kg)	Medium sand (g/kg)	Fine sand (g/kg)	Very fine sand (g/kg)	Silt (g/kg)	Coarse silt (g/kg)	Fine silt (g/kg)	Clay (g/kg)	T ²	CS/MS ³	D ⁴ (%)	CS/FS ⁵	D ⁶ (%)	MS/FS ⁷	D ⁸ (%)
P1 Alice Lake – Cambisol (Humic, Loamic)																		
A1	0–15	592	47	90	287	14	154	332	194	138	76	SL	0.3	17.8	6.4	183	20.3	243
2A2	15–28	539	50	92	241	41	116	374	170	204	87	SL	0.4	9.3	2.3	15	5.9	6.3
2Bw	28–43	515	57	92	219	35	112	380	164	216	105	L	0.4	5.4	2.6	35.6	6.3	38.9
3Cox/Bw	43–70+	761	82	149	374	36	119	172	89	83	68	LS	0.4	–	4.1	–	10.3	–
P2 Temple Lake – Protostagnic Cambisol (Humic, Loamic, Raptic)																		
A	0–17	529	66	96	202	86	79	335	109	226	136	SL	0.5	32.3	1.1	51	2.3	14.1
2Bwg1	17–40	428	33	59	162	79	95	386	158	228	186	L	0.4	7.8	0.7	15.9	2.1	22
3Bwg2	40–78+	590	59	90	268	102	71	354	137	217	56	SL	0.3	–	0.9	–	2.6	–
P3 Lonesome Lake – Entic Podzol (Arenic)																		
O	0–5	–	–	–	–	–	–	–	–	–	–	–	–	–	–	–	–	–
A	5–17	263	32	42	70	36	84	348	130	218	389	CL	0.6	17.2	1.2	29.1	2	14.4
2EB	17–30	408	58	89	124	54	82	367	168	199	226	L	0.7	32	1.7	55.7	2.3	17.9
3Bs	30–45	709	96	119	218	112	165	289	162	128	2	LS	0.5	16.2	1.1	11.8	2	5.3
3Cox/B	45–55+	789	124	137	209	113	205	208	93	115	3	LS	0.7	–	1.2	–	1.9	–

¹ Sand = 2000–63 µm; Very coarse sand = 2000–1250 µm; Coarse sand = 1250–630 µm; Medium sand = 630–200 µm; Fine sand = 200–125 µm; Very fine sand = 125–63 µm; Silt = 63–2 µm; Coarse silt = 63–20 µm; Fine silt = 20–2 µm; Clay = <2 µm.

² T = Textural class; LS = Loamy sand; SL = Sandy loam; L = Loam; CL = Clay loam.

³ Ratio of coarse sand to medium sand.

⁴ Difference in the ratio of coarse sand to medium sand for the underlying and overlying horizon.

⁵ Ratio of coarse sand to medium sand.

⁶ Difference in the ratio of coarse sand to medium sand between the underlying and overlying horizon.

⁷ Ratio of medium sand to fine sand.

⁸ Difference in the ratio of coarse sand to medium sand between the underlying and overlying horizon.

4.2. Soil morphological and physical characteristics

Soils on moraines in the Cirque of the Towers have developed on granitic till. All soils are acidic with a pH in the range of 4.3 to 5.0 in the topsoil, have a high organic carbon content in their uppermost horizons and show a trend of increasing bulk density with depth (Table 3). Bulk density values of 0.8 to 1.0 g/cm³ are rather low in the upper horizon of the soils due to the low soil skeleton proportion. In addition, organic matter is present to a relatively great depth which contributes to the low bulk densities. All investigated soils exhibit two lithological discontinuities that was evidenced by a textural change and an increase in coarse fragments with depth (Table 4).

Profiles P1 (Alice Lake moraine) and P2 (Temple Lake moraine) are classified as Cambisols (Reference Soil Group–RSG). In profile P1, the content of coarse fragments (>2 mm) increases with depth, from about 5% in the A1 horizon to about 38% in the 3Cox/Bw horizon. The A1 and 2A2 horizons have sandy loam textures and the 2Bw horizon is loam and the 3Cox/Bw horizon is loamy sand (Tables 3 and 4). P1 has fine roots in all horizons.

The profile P2 is better developed with a thicker B horizon. The cambic horizon exhibits weakly expressed stagic properties, in which redoximorphic features (Fe mottling) make up a minor portion of the soil volume (Table 4). In contrast to P1, profile P2 predominantly has fine and medium roots.

Profile P3 is classified as Entic Podzol (Arenic). It presents a weakly-moderately developed 3Bs horizon that fulfils, at least partially, the requirements of a spodic horizon with the colour (7.5YR4/6), pH (5.0) and organic carbon content (12 g/kg). It has a transitional EB horizon that overlies the Bs horizon. P3 exhibits a high abundance of fine, medium and coarse roots that are concentrated in the A and 2EB horizons (Table 3).

Similarly to the vegetation cover (Table 1), the abundance of roots in the soils (Table 3) increased from profile 1 to profile 3.

4.3. ²⁴⁰Pu/²³⁹Pu ratio and ²³⁹⁺²⁴⁰Pu inventories

The distribution of the ²⁴⁰Pu/²³⁹Pu atomic ratios for all samples (reference and erosion sites) exhibits slight increases with depth: 0–5 cm = 0.15 ± 0.02; 5–10 cm = 0.17 ± 0.02; 10–15 cm = 0.20 ± 0.05; 15–20 cm = 0.19 ± 0.04. In general, the ²³⁹⁺²⁴⁰Pu activities of all reference and erosion sites show the same distribution trend with depth: Pu activities are higher at the soil surface (0–5 cm) and decrease exponentially with depth (Fig. 2). Only the erosional site at Temple Lake shows a relatively high ²³⁹⁺²⁴⁰Pu activity at 10–15 cm, but having also a large error range.

Compared to the reference sites, the erosion sites of the Alice Lake and Temple Lake moraines exhibit lower total Pu inventories. This is not the case for the Lonesome Lake site, where the erosional and reference sites exhibit similar values (Fig. 2).

4.4. Rates of soil erosion and accumulation

The ²³⁹⁺²⁴⁰Pu inventories on these moraines clearly indicate a considerable decrease in net soil erosion with increasing age, regardless of the model used (Fig. 3). The Pu inventories in fact indicate an overall mass loss or gain and, thus, a change in mass of a specific soil. The change in the Pu inventory or soil mass (M) is given by:

$$\frac{dM}{dt} = D(t) - E(t) - L(t) \quad (5)$$

with $D(t)$ = dust input, $E(t)$ = erosion rate, $L(t)$ = leaching rate. Due to the insolubility of Pu, leaching rates can be assumed to be negligible.

Soils on the Alice Lake (P1) and Temple Lake (P2) moraines show negative values that indicate more soil erosion than accumulation. Both of these tundra sites show high mass losses and thus net erosion rates (values range from 517 to 257 t/km²/a and 172 to 72 t/km²/a). The forested site on the Lonesome Lake moraine exhibits values that are close to zero or slightly positive, indicating some minor soil accumulation (rates between 15 and 48 t/km²/a). Higher net rates (erosion, accumulation) were obtained for all sites when using the IM with the particle size correction factor $P = 1$, when compared to factors of $P = 1.2$ or $P = 1.5$ (Fig. 3). When we applied the PDM model to the ²³⁹⁺²⁴⁰Pu data, the soil erosion rates generally followed the same trend with time. The erosion rate was higher for the Alice Lake profile (average of 517 t/km²/a) and lower for the Temple Lake profile (average of 72 t/km²/a).

4.5. Correlation between soil organic carbon and $\delta^{13}C$

The $\delta^{13}C$ values for the reference sites on the Alice Lake and Temple Lake moraines generally increased with depth and ranged between -28‰ and -24‰ . The $\delta^{13}C$ values varied less in the profile on the Lonesome Lake moraine. The erosion site on the Alice Lake moraine showed a similar trend, but with less variation. The erosion site on the Temple Lake moraine shows an inversion of the 0–5 cm and 5–10 cm samples. $\delta^{13}C$ values from soil horizons at the reference and erosional sites on the Lonesome Lake moraine are generally similar, but the erosional site shows more variability.

Surprisingly, the correlation between SOC% and $\delta^{13}C$ becomes weaker at all reference and erosion sites on older moraines (Fig. 4). Overall, the tundra reference sites show negative correlations between SOC and $\delta^{13}C$. Among all sites, the reference site on the Alice Lake moraine has the highest correlation ($R^2 = 0.88$) while the correlation for the corresponding erosional site is only $R^2 = 0.34$. The Temple Lake moraine shows a moderately negative correlation at the reference site ($R^2 = 0.51$) and a very weak positive correlation at the erosional site ($R^2 = 0.13$). At Lonesome Lake, the most notable pattern is seen in the noticeably higher SOC value of the 0–5 cm samples when compared to the subsurface (especially in the reference profile).

5. Discussion

5.1. Onset of soil formation

The ¹⁰Be surface exposure dating provided an updated chronology for the moraines in the Cirque of the Towers (WRR) and, therefore, the timing for the onset of soil formation. Our results indicate that some of these moraines are older than previously estimated (Dahms et al., 2010). The Alice Lake moraine now appears to correspond to the IACP-Younger Dryas cooling event and not to a Holocene 'Neoglacial' period as previously reported (Dahms et al., 2010). The Temple Lake and Lonesome Lake moraines now appear to be roughly coeval to the Oldest Dryas (Shakun and Carlson, 2010), although the period of glacier recession and re-advance between 15 and 18 ka may more properly be termed 'pre-Bølling-Allerød' (Rasmussen et al., 2014). These are so far some of the very few numerical dating attempts of lateglacial moraines in the Wind River Range. The Temple Lake and Lonesome Lake moraines, although separated over a relatively long distance (approximately 1 km), also represent several re-advance phases during the Oldest Dryas. However, the term 'Oldest Dryas' is poorly defined and should, according to Rasmussen et al. (2014), not be used. This episode was defined as a period of biostratigraphic change reflected in terrestrial records in Denmark (Iversen, 1954). The period between 15 and 18 ka belongs to a general period with glacier recession and re-advances.

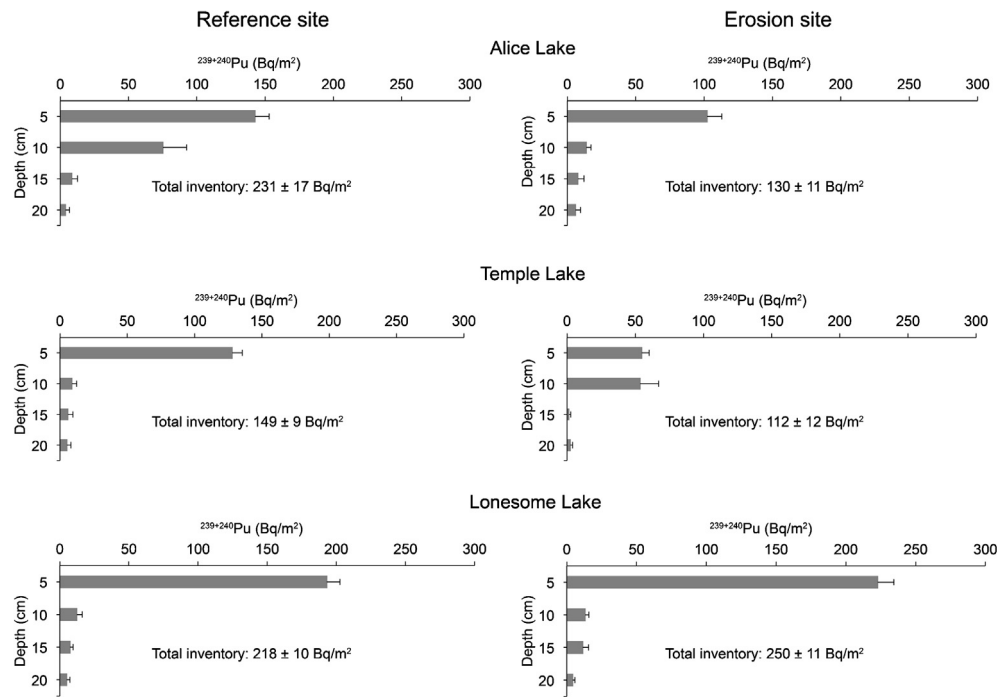


Fig. 2. Average $^{239+240}\text{Pu}$ activity (\pm standard error) with soil depth and total inventory of the reference and erosional sites along the investigated sequence.

The moraines we sampled in Cirque of the Towers correspond to the pre- Bølling–Allerød and IACP–Younger Dryas cooling phases and, at least in the investigated valley, deposits corresponding to a Holocene ‘Neoglacial’ cold period are no longer identified (Dahms et al., 2018).

5.2. Provenance and distribution of Pu isotopes

Surface soils (0–5 cm), containing the majority of the $^{239+240}\text{Pu}$ inventory, exhibited $^{240}\text{Pu}/^{239}\text{Pu}$ ratios of (0.15 ± 0.02) , which appear to be slightly lower than the well-established global fallout range of 0.18 ± 0.014 for Northern Hemisphere mid-latitude fallout (Kelley et al., 1999). The data indicate a mixing between global fallout and tropospheric fallout originating from the Nevada Test Site fallout. Previous work in the western US (Ketterer et al., 2004) has demonstrated the presence of similar mixing in locations Nevada, Arizona and Utah. In general, the distribution of $^{239+240}\text{Pu}$ activities in our reference profiles is consistent with reported trends in the literature where higher activity is found at the soil surface exponentially decreasing with depth (Ketterer et al., 2004; Meusburger et al., 2016; Zollinger et al., 2015).

The total $^{239+240}\text{Pu}$ inventories did not change along the investigated chronosequence and showed an average value close to 200 Bq/m^2 . Plutonium is strongly retained in the upper 5 cm of the soils. Pu isotopes have a high ionic potential and strongly associate with specific soils phases such as iron/manganese oxides and humic substances (Ketterer et al., 2011). Because of the sizeable accumulation of organic matter in the A horizons, the potential translocation of Pu with percolating soil water appears to be strongly limited in these soils. As a consequence, a correlation between Pu and org. C was found (Fig. 4; all sites). Due to stronger disturbances at the erosional sites, this correlation was weaker. Furthermore, the $^{239+240}\text{Pu}$ inventories that we measure in Cirque of the Towers are slightly higher than in other mountain regions in the Swiss Alps where about $80\text{--}100 \text{ Bq/m}^2$ is often measured (Meusburger et al., 2016; Zollinger et al., 2015). The enhanced $^{239+240}\text{Pu}$ inventories in the Wind River Basin are not unexpected, and could arise from the additional NTS input, as well

as local/regional differences in local climate and precipitation patterns.

5.3. Evolution of soil erosion rates

The rates of soil erosion that we calculated for these soils declined noticeably with continued soil development over time and increased vegetation cover associated with natural successional changes. With the development of tundra and forest vegetation, soil erodibility apparently was drastically reduced. Vegetation and the observed changes in roots (density and thickness) certainly contributed to the decrease in erosion with increasing soil age. The measured rates of soil erosion for the younger soils (Cambisols) are comparable with Alpine soils that have developed in the active layer of permafrost (Zollinger et al., 2015). On the Alice Lake moraine, the erosion rates are in the range of 260 to $520 \text{ t km}^{-2} \text{ a}^{-1}$. These are rather high values for natural and not human-affected alpine sites (Alewell et al., 2014; Zollinger et al., 2015). The observed changes in the vegetation type and cover (Table 1) certainly contributed to the decrease in erosion with increasing soil age.

The slightly positive values at the Lonesome Lake suggest both that the surface became stable and that the rates of dust accumulation outpaced erosion rates. Dust accumulation on soils have been reported in the WRR and its deposition is not only related to glacial episodes but is an ongoing process even in the post-glacial period (Applegarth and Dahms, 2004; Dahms and Rawlins, 1996). Dahms and Rawlins (1996) measured rates of modern dust deposition in the western slope of the WRR between 0.23 to $31.0 \times 10^{-7} \text{ g cm}^{-2} \text{ d}^{-1}$ for mineral dust which corresponds to 0.08 to $11.32 \text{ t km}^{-2} \text{ a}^{-1}$. These rates have to be considered as minimum values, because the organic fraction was not included in their measurements. Brahney et al. (2015) inferred dust deposition rates for the last 2000 yrs of $0\text{--}4 \text{ t km}^{-2} \text{ a}^{-1}$ from lake sediments of two lakes in the Wind River Range. Apparently due to human impact, deposition rates at Lonesome Lake and North Lake increased to 25 and 58 t km^{-2} , respectively, during the last few decades. Our measured soil accumulation rates at the Lonesome Lake site are in the range of 10 to $48 \text{ t km}^{-2} \text{ a}^{-1}$. These values are close to the

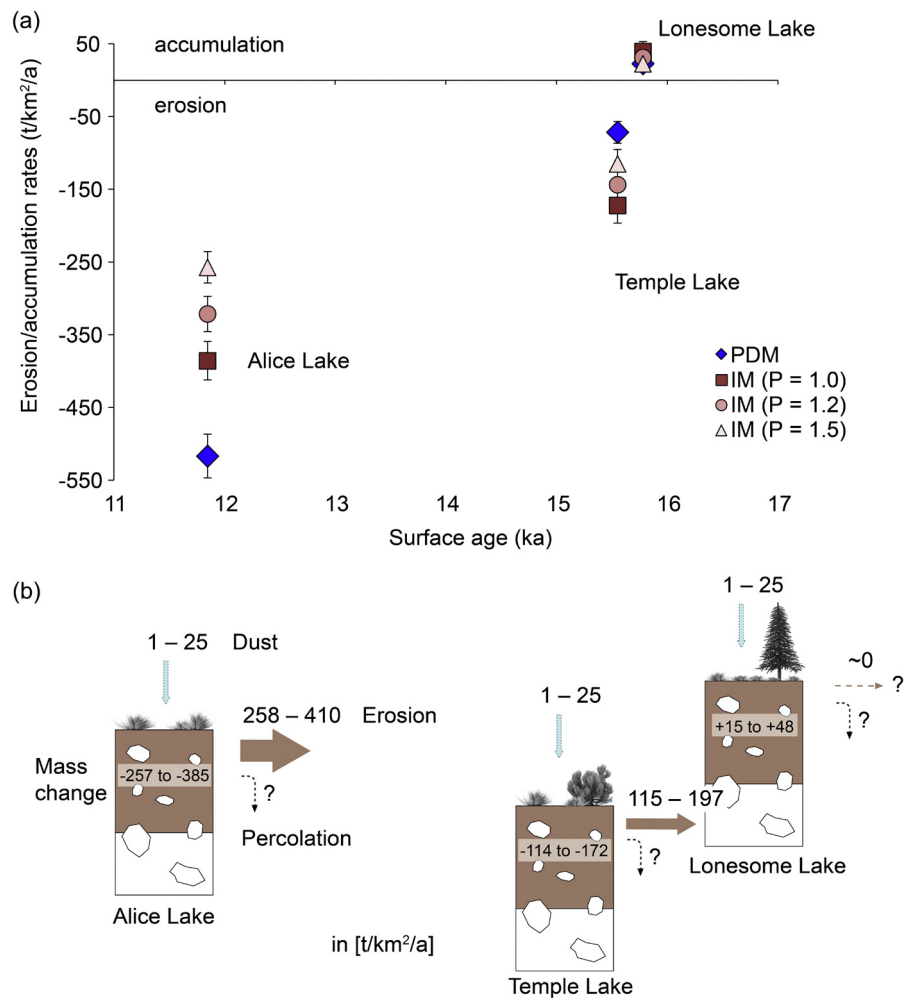


Fig. 3. (a) Soil erosion and accumulation rates of the moraine study sites as a function of surface age. Negative values indicate soil erosion and positive values soil accumulation. The rates were calculated using the $^{239+240}\text{Pu}$ inventories, the Profile Distribution Model (PDM) (Walling and Quine, 1990; Zhang et al., 1990) and the Inventory Model (IM) (Lal et al., 2013). The following particle size correction factors were considered: $P = 1$ and $P = 1.2$ (according to Walling and He, 1999) and $P = 1.5$ (according to Lal et al., 2013). (b) Calculated mass fluxes in and out of the soils using the inventory method ($P = 1$ to 1.5) and estimated dust deposits (based on Dahms and Rawlins, 1996 and Brahney et al., 2015). See also equation (5).

dust deposition rates determined by Dahms and Rawlins (1996) and Brahney et al. (2015). This furthermore suggests that the soils on the moraine slopes have little detectable erosion now, but receive some aeolian input that gives rise to a slightly positive mass balance. After more than 12 ka soil evolution, the moraine slopes have therefore become stabilised and may even exhibit a positive mass balance.

The $\delta^{13}\text{C}$ -signature in topsoil layers showed values within the typical range of C_3 -plants (-20 to -30‰). Several studies have reported a close correlation between $\delta^{13}\text{C}$ and soil organic carbon at undisturbed sites, with an enrichment of ^{13}C with soil depth (Alewell and Schaub, 2009; Meusburger et al., 2013; Zollinger et al., 2015). In general, a better relationship between total soil organic carbon (SOC) and $\delta^{13}\text{C}$ was obtained at the reference sites than at the erosional sites (Fig. 4). This indeed indicates that the distribution pattern of $\delta^{13}\text{C}$ and total SOC was at least partially influenced by slope mass movement at the erosion sites. As the relative proportion of ^{13}C and ^{12}C changes due to fractionation processes during the decomposition of SOC, SOC consequently becomes enriched in ^{13}C relative to ^{12}C as decomposer organisms preferentially utilise the lighter isotopic species, which has a lower dissociation energy and therefore requires less energy to be broken from their molecules (Alewell and Schaub, 2009). Furthermore, our results provide evidence that the relationship of SOC and $\delta^{13}\text{C}$

weakens with soil age, i.e. from profile P1 to P3. This is a surprising result as we expected the contrary trend. We show that erosion rates distinctly decrease with soil age (Fig. 3). Consequently, a better correlation between $\delta^{13}\text{C}$ and SOC should be expected at both the reference and ‘erosional’ sites (Zollinger et al., 2015). The approach of SOC and $\delta^{13}\text{C}$ gives, at its best, only qualitative indications about soil erosion. The unexpected trend seems to contradict the Pu-results. Thus the erosion signal in the $\delta^{13}\text{C}$ data must have been erased by other processes over time. With increasing time and stabilisation of the slopes, the distribution of organic carbon and $\delta^{13}\text{C}$ along the profile should approach a quasi-steady state situation that follows a clear depth pattern and thus close relation between org. C and $\delta^{13}\text{C}$ (Poage and Feng, 2004). This is, however, not the case and might be due either to increased bioturbation with increasing soil age or an increased accumulation of aeolian material with time that changes the relationship between SOC and $\delta^{13}\text{C}$. Over a longer-term, cryoturbation may also disturb the $\delta^{13}\text{C}$ distribution. Cryogenesis is often the controlling factor in patterned ground formation which also results in cryoturbated soil profiles, cryostructures and carbon sequestration (Ping et al., 2008). Plutonium integrates mass movements for the last about 5 decades whereas carbon isotopes cover a longer time period (up to century or even millennia). Therefore, carbon isotopes may also re-

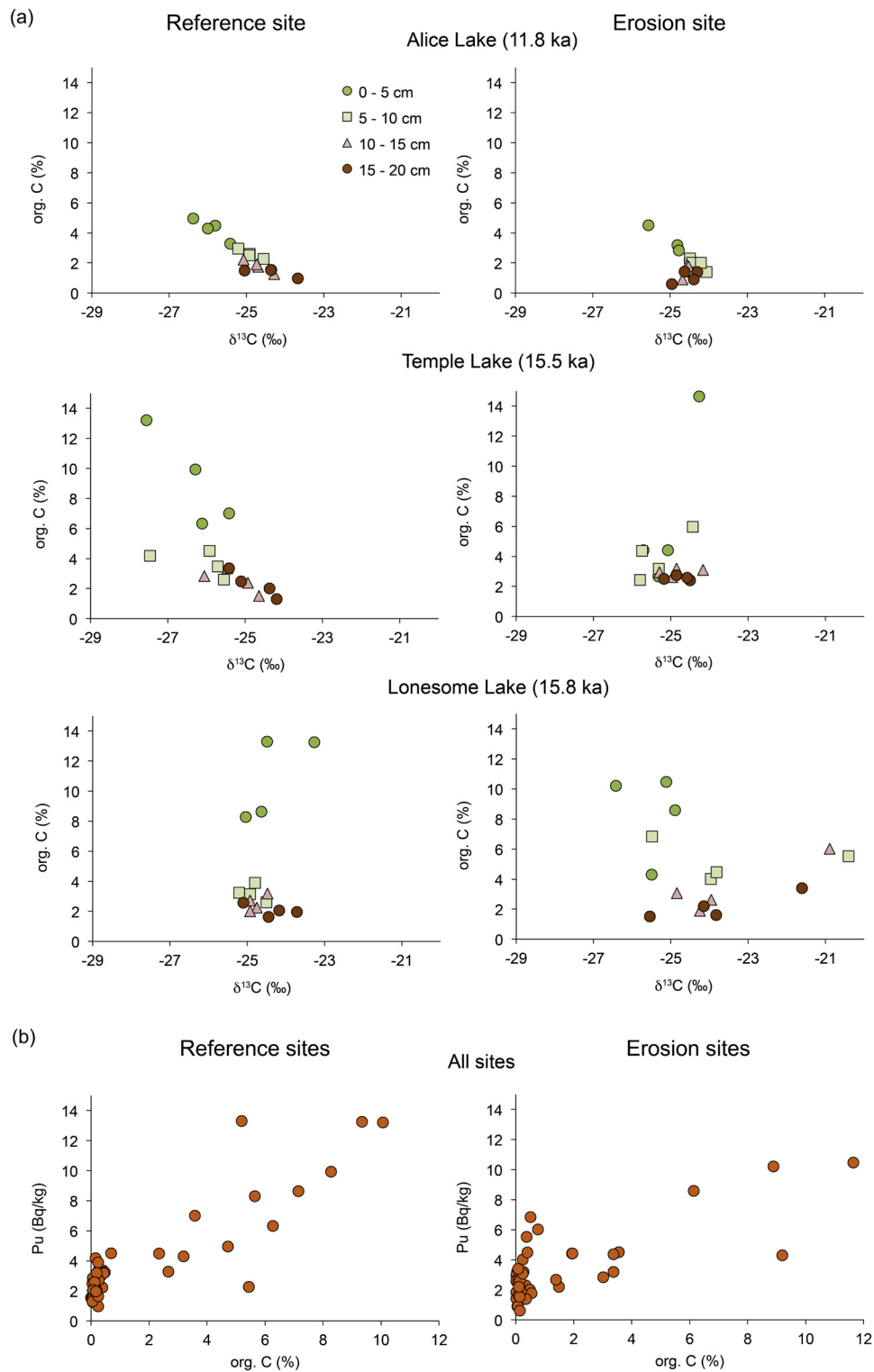


Fig. 4. (a) Comparison between soil organic carbon (SOC) content and $\delta^{13}\text{C}$ of the soil samples at the reference and erosion/accumulation sites and as function of sampling depth. (b) Correlation of $^{239+240}\text{Pu}$ with organic C at the reference and erosion/accumulation sites.

flect processes other than only erosion (Alewell and Schaub, 2009; Alewell et al., 2014).

5.4. Soil evolution since the late Pleistocene

In general, the soils showed greater profile differentiation and a higher degree of rubification and consistency (Table 3) with increasing age. These trends are consistent with results obtained in

previous studies from the WRR (Dahms, 2002; Dahms et al., 2012). Furthermore, the soil evolutionary pathway – from Lithosols to Cambisols towards Podzols – found here is similar to those in European cold alpine environments (Dahms et al., 2012). Due to the higher levels of precipitation and lower rates of dust deposition, Podzols in the European Alps require much less time to develop than in the WRR (Dahms et al., 2012).

Dahms (2002) and Dahms et al. (2010) studied soils elsewhere in the WRR and demonstrated that soils on Temple Lake moraines usually present a slightly higher degree of development (e.g. in terms of the silt and clay content) than Alice Lake moraine soils. Usually, argic horizons were reported for Temple Lake soils. The profiles P1 and P2 did not present a typical Bt horizon. According to Birkeland (1984), aeolian input in gravelly parent materials (e.g. till) accelerates the formation of Bt horizons because the fine particles can easily infiltrate and accumulate downward in the soil profile. This process results in a well-known feature in some alpine soils of the Rocky Mountains, the so-called ‘mixed loess’ (Shroba and Birkeland, 1983). However, this feature could also be due to layering. In an allocthonous approach, relatively sharp boundaries within soil profiles, marking abrupt changes in soil physical and chemical properties, frequently originate from discontinuities rather than exclusively from pedogenic processes (Lorz et al., 2013). Soils formed in cover-bed successions have layered parent materials with such discontinuities.

The presence of lithological discontinuities in all soil profiles, evidenced by a change in the coarse fragment content and in the sand fractions, suggests that they have formed two different parent materials. The following processes may have been the cause for the formation of these lithological discontinuities:

- i) Aeolian input: due to the relatively dry conditions in the whole mountain range and surroundings, dust input is quite common (Dahms and Rawlins, 1996). In addition, some local loess input during deglaciation also might have been possible. Although there is no distinct loess layer covering the soils (because of aeolian fines being mixed into the till), it might be possible that the A and 2B horizons which exhibit a higher proportion of silt and clay content than their underlying horizons (Table 4) have been overprinted by dust input giving rise to stratification.
- ii) The soils may have lost part of their upper horizons by erosion episodes during periods of cold desiccating conditions (Younger Dryas or later stadials during the Holocene) with scarce deposition (see also Hall, 1999). A later period of deposition of a second type of material on top of the soil gives rise to an additional lithological discontinuity. However, this remains slightly hypothetical because till often is layered.

Hence, the substrate of P1, P2 and P3 was formed by a sequence of different processes that are typical for glacial and paraglacial environments. The glacial till was covered by sandy and silty sediments having a gravel content of <10%. This sandy-silty sediment has an aeolian origin and was partially mixed with the pre-existent till substrate, e.g., due to periglacially induced near-surfaces processes.

Erosion rates are very high at site P1. Nonetheless, the rate of pedogenesis was still sufficient to form a shallow Cambisol about 40 cm thick. Over time, the strong soil erosion caused less-weathered substrate to come closer to the land surface, so that soil is continuously rejuvenated. Due to the earlier stabilisation of the land surface by vegetation and roots at P3, soil erosion rates are now lower than accumulation rates (Fig. 3). This stabilisation could explain the difference to site P2, where a Cambisol developed instead of a Podzol.

6. Conclusions

We provide in this study the first description and quantification of the temporal evolution of soil erosion and consequent stabilisation of moraine slopes in an alpine region. Our results support the hypothesis that soil erosion rates decrease over time as soils develop. Weakly to moderately developed soils (Cambisols)

on younger moraines under tundra vegetation show evidence of high erosion rates (260 to 520 t km⁻² a⁻¹) whereas the soils (Podzol) on the older moraines under forest vegetation exhibit erosion rates that are close to zero or even slightly positive – indicating some weak net accumulation. Moraine slopes in the study area, therefore, apparently reach geomorphological stability after more than 12 ka of soil formation. After this time, soil erosion rates reach nearly zero and soils even seem to receive a slight excess input due to dust accumulation. Furthermore, we provide an updated chronology for the glacial deposits in the Cirque of the Towers (WRR) that indicates that they have to be associated to the Lateglacial (post-LGM) period.

The correlation between $\delta^{13}\text{C}$ and SOC shows that bioturbation and/or dust input becomes more effective with time. This is possibly why the expected increase in correlation between $\delta^{13}\text{C}$ and org. C was not detected. Erosion caused soil rejuvenation during the early stages of soil development; but with time, and after stabilisation of the slopes, aeolian input then comes to dominate soil formation and leads to the development of a positive mass balance.

Acknowledgements

This research was supported by the Swiss Government Excellence Scholarship (2016.0646/Brazil/OP) for Raquel Portes and by the Foundation for Research in Science and the Humanities at the University of Zurich (grant number STWF-17-025). We thank Sandro Egli for the assistance during the fieldwork and Diogo Noses Spinola for comments and proofreading of the manuscript. Sampling was performed in the Washakie District of Shoshone National Forest under Special Use Permit #2037-01. We also thank two unknown reviewers for their useful comments on an earlier version of the manuscript.

References

- Alewel, C., Meusburger, K., Juretzko, G., Mabit, L., Ketterer, M.E., 2014. Suitability of ²³⁹⁺²⁴⁰Pu and ¹³⁷Cs as tracers for soil erosion assessment in mountain grasslands. *Chemosphere* 103, 274–280. <https://doi.org/10.1016/j.chemosphere.2013.12.016>.
- Alewel, C., Schaub, M., 2009. Stable carbon isotopes and oxygen isotopes as an indicator for soil degradation. *Rapid Commun. Mass Spectrom.* 24, 3567–3577. <https://doi.org/10.1002/rcm>.
- Applegarth, M.T., Dahms, D., 2004. Aeolian modification of moraine soils, Whiskey Basin, Wyoming, USA. *Earth Surf. Process. Landf.* 29, 579–585. <https://doi.org/10.1002/esp.1052>.
- Balco, G., Stone, J.O., Lifton, N.A., Dunai, T.J., 2008. A complete and easily accessible means of calculating surface exposure ages or erosion rates from ¹⁰Be and ²⁶Al measurements. *Quat. Geochronol.* 3, 174–195.
- Birkeland, P.W., 1984. *Soils and Geomorphology*. Oxford University Press, New York.
- Bockheim, J.G., 1980. Solution and use of chronofunctions in studying soil development. *Geoderma* 24, 71–85.
- Brahney, J., Ballantyne, A.P., Kocielek, P., Leavitt, P.R., Farmer, G.L., Neff, J.C., 2015. Ecological changes in two contrasting lakes associated with human activity and dust transport in western Wyoming. *Limnol. Oceanogr.* 60, 678–695.
- Chmeleff, J., von Blanckenburg, F., Kossert, K., Jakob, D., 2010. Determination of the ¹⁰Be half-life by multicollector ICP-MS and liquid scintillation counting. *Nucl. Instrum. Methods Phys. Res., Sect. B* 268, 192–199.
- Christl, M., Vockenhuber, C., Kubik, P.W., Wacker, L., Lachner, J., Alfmov, V., Synal, H.-A., 2013. The ETH Zurich AMS facilities: performance parameters and reference materials. *Nucl. Instrum. Methods Phys. Res., Sect. B, Beam Interact. Mater. Atoms* 294, 29–38.
- Dahms, D.E., 2002. Glacial stratigraphy of Stough Creek Basin, Wind River Range Wyoming. *Geomorphology* 42, 59–83.
- Dahms, D.E., Rawlins, C.L., 1996. A two-year record of eolian sedimentation in the Wind River Range, Wyoming, USA. *Arct. Alp. Res.*, 210–216.
- Dahms, D., Egli, M., Fabel, D., Harbor, J., Brandova, D., Portes, R.C., Christl, M., 2018. Revised Quaternary glacial succession and post-LGM recession, southern Wind River Range, Wyoming, USA. *Quat. Sci. Rev.* 192, 167–184. <https://doi.org/10.1016/j.quascirev.2018.05.020>.
- Dahms, D., Favilli, F., Krebs, R., Egli, M., 2012. Soil weathering and accumulation rates of oxalate-extractable phases derived from alpine chronosequences of up

- to 1 Ma in age. *Geomorphology* 151–152, 99–113. <https://doi.org/10.1016/j.geomorph.2012.01.021>.
- Dahms, D.E., Birkeland, P.W., Shroba, R.R., Miller, C.D., 2010. Latest Quaternary glacial and periglacial stratigraphy, Wind River Range, Wyoming. *Geological Society of America Digital Map and Chart Series*, <https://doi.org/10.1130/2010.DMCH007.TXT>.
- FAO, 2006. *Guidelines for Soil Description*, 4th ed. Rome.
- Gosse, J.C., Phillips, F.M., 2001. Terrestrial in situ cosmogenic nuclides: theory and application. *Quat. Sci. Rev.* 20, 1475–1560.
- Hall, R.D., 1999. Effects of climate change on soils in glacial deposits, Wind River Basin, Wyoming. *Quat. Res.* 51, 248–261. <https://doi.org/10.1006/qres.1999.2032>.
- He, Q., Walling, D.E., 1997. The distribution of fallout ^{137}Cs and ^{210}Pb in undisturbed and cultivated soils. *Appl. Radiat. Isot.* 48, 677–690.
- He, Q., Walling, D.E., 1996. Interpreting particle size effects in the adsorption of ^{137}Cs and unsupported ^{210}Pb by mineral soils and sediments. *J. Environ. Radioact.* 30, 117–137.
- Huggett, R.J., 1998. Soil chronosequences, soil development, and soil evolution: a critical review. *Catena* 32, 155–172. [https://doi.org/10.1016/S0341-8162\(98\)00053-8](https://doi.org/10.1016/S0341-8162(98)00053-8).
- IUSS Working Group WRB, 2014. *World Reference Base for Soil Resources*. World Soil Resources Reports. Rome.
- Iversen, J., 1954. The late-glacial flora of Denmark and its relation to climate and soil. *Danmarks Geologiske Undersøgelser, Række II*, 80.
- Keefer, W.R., 1970. *Structural Geology of the Wind River Basin, Wyoming*.
- Kelley, J.M., Bond, L.A., Beasley, T.M., 1999. Global distribution of Pu isotopes and ^{237}Np . *Sci. Total Environ.* 237–238, 483–500.
- Ketterer, M.E., Hafer, K.M., Link, C.L., Kolwaite, D., Wilson, J., Mietelski, J.W., 2004. Resolving global versus local/regional Pu sources in the environment using sector ICP-MS environment using sector ICP-MS. *J. Anal. At. Spectrom.* 19, 241–245.
- Ketterer, M.E., Zheng, J., Yamada, M., 2011. Applications of transuranics as tracers and chronometers in the environment. In: Baskaran, M. (Ed.), *Handbook of Environmental Isotope Geochemistry*. Springer, p. 944.
- Kohl, C., Nishiizumi, K., 1992. Chemical isolation of quartz for measurement of in situ-produced cosmogenic nuclides. *Geochim. Cosmochim. Acta* 56, 3583–3587. [https://doi.org/10.1016/0016-7037\(92\)90401-4](https://doi.org/10.1016/0016-7037(92)90401-4).
- Lal, R., Elliot, W., 1994. Erodibility and erosivity. In: Lal, R. (Ed.), *Soil Erosion Research Method*. Soil Water Conserv. Soc., St. Lucie Press, Delray Beach, Florida, pp. 181–208.
- Lal, R., Wasson, R., Tims, S.G., 2013. Applicability of ^{239}Pu as a tracer for soil erosion in the wet-dry tropics of northern. *Nucl. Inst. Methods Phys. Res. B* 294, 577–583. <https://doi.org/10.1016/j.nimb.2012.07.041>.
- Lorz, C., Frühauf, M., Mailänder, R., Phillips, J.D., Kleber, A., 2013. Influence of cover beds on soils. In: Kleber, A., Terhorst, B. (Eds.), *Mid-Latitude Slope Deposits (Cover Beds)*. In: *Dev. Sedimentol.*, vol. 66, pp. 95–125.
- Masarik, L., Wieler, R., 2003. Production rates of cosmogenic nuclides in boulders. *Earth Planet. Sci. Lett.* 216, 201–208.
- Meusbürger, K., Mabit, L., Ketterer, M., Park, J.H., Sandor, T., Porto, P., Alewell, C., 2016. A multi-radionuclide approach to evaluate the suitability of $^{239+240}\text{Pu}$ as soil erosion tracer. *Sci. Total Environ.* 566–567, 1489–1499. <https://doi.org/10.1016/j.scitotenv.2016.06.035>.
- Meusbürger, K., Mabit, L., Park, J.H., Sandor, T., Alewell, C., 2013. Combined use of stable isotopes and fallout radionuclides as soil erosion indicators in a forested mountain site, South Korea. *Biogeosciences* 10, 5627–5638. <https://doi.org/10.5194/bg-10-5627-2013>.
- Muhs, D., 2013. The geologic record of dust in the Quaternary. *Aeolian Res.* 9, 3–48.
- Nishiizumi, K., Imamura, M., Caffee, M.W., Southon, J.R., Finkel, R.C., McAninch, J., 2007. Absolute calibration of ^{10}Be AMS standards. *Nucl. Instrum. Methods Phys. Res., Sect. B, Beam Interact. Mater. Atoms* 258, 403–413. <https://doi.org/10.1016/j.nimb.2007.01.297>.
- Pigati, J.S., Lifton, N.A., 2004. Geomagnetic effects on time-integrated cosmogenic nuclide production with emphasis on in situ ^{14}C and ^{10}Be . *Earth Planet. Sci. Lett.* 226, 193–205.
- Ping, C.L., Michaelson, G.J., Kimble, J.M., Romanovsky, V.E., Shur, Y.L., Swanson, D.K., Walker, D.A., 2008. Cryogenesis and soil formation along a bioclimate gradient in Arctic North America. *J. Geophys. Res., Biogeosci.* 113, G03S12.
- Poage, M.A., Feng, X., 2004. A theoretical analysis of steady state $\delta^{13}\text{C}$ profiles of soil organic matter. *Glob. Biogeochem. Cycles* 18, GB2016. <https://doi.org/10.1029/2003GB002195>.
- Quine, T.A., Walling, D.E., 1991. Rates of soil erosion on arable fields in Britain: quantitative data from caesium-137 measurements. *Soil Use Manage.* 7, 169–176.
- Rasmussen, S.O., Bigler, M., Blockley, S.P., Blunier, T., Buchardt, S.L., Clausen, H.B., Cvijanovic, I., Dahl-Jensen, D., Johnsen, S.J., Fischer, H., Gkinis, V., Guillevic, M., Hoek, W.Z., Lowe, J.L., Pedro, J.B., Popp, T., Seierstad, I.K., Steffensen, J.P., Svensson, A.M., Vallelonga, P., Vinther, B.M., Walker, M.J.C., Wheatley, J.J., Winstrup, M., 2014. A stratigraphic framework for abrupt climatic changes during the Last Glacial period based on three synchronized Greenland ice-core records: refining and extending the INTIMATE event stratigraphy. *Quat. Sci. Rev.* 106, 14–28.
- Schaetzl, R.J., 1998. Lithologic discontinuities in some soils on drumlins: theory, detection, and application. *Soil Sci.* 16, 570–590.
- Shakun, J.D., Carlson, A.E., 2010. A global perspective on Last Glacial Maximum to Holocene climate change. *Quat. Sci. Rev.* 29, 1801–1816.
- Shroba, R.R., Birkeland, P.W., 1983. Trends in late-Quaternary soil development in the Rocky Mountains and Sierra Nevada of the western United States. In: Porter, S.C. (Ed.), *Late-Quaternary Environments of the United States*. University of Minnesota Press, Minneapolis.
- Stone, J.O., 2000. Air pressure and cosmogenic isotope production. *J. Geophys. Res., Solid Earth* 105, 23753–23759.
- von Blanckenburg, F., Belshaw, N.S., O’Nions, R.K., 1996. Separation of ^9Be and cosmogenic ^{10}Be from environmental materials and SIMS isotope dilution analysis. *Chem. Geol.* 129, 93–99.
- Walling, D., He, Q., 1999. Improved models for estimating soil erosion rates from caesium-137 measurements. *J. Environ. Qual.* 28, 611–622.
- Walling, D., Quine, T., 1990. Calibration of caesium-137 measurements to provide quantitative erosion rate data. *Land Degrad. Rehabil.* 2, 161–175.
- Whittaker, R.H., 1962. Classification of natural communities. *Bot. Rev.* 28, 1–239.
- Wischmeier, W.H., Smith, D.D., 1960. A universal soil loss estimating equation to guide conservation farm planning. In: *Proceedings of the 7th International Congress of Soil Science*, vol. 1, pp. 418–425.
- Zhang, X., Higgitt, D.L., Walling, D.E., 1990. A preliminary assessment of the potential for using caesium-137 to estimate rates of soil erosion in the Loess Plateau of China. *Hydrol. Sci. J.* 35, 43–252.
- Zollinger, B., Alewell, C., Kneisel, C., Meusbürger, K., Brandová, D., Kubik, P., Schaller, M., Ketterer, M., Egli, M., 2015. The effect of permafrost on time-split soil erosion using radionuclides (^{137}Cs , $^{239+240}\text{Pu}$, meteoric ^{10}Be) and stable isotopes ($\delta^{13}\text{C}$) in the eastern Swiss Alps. *J. Soils Sediments* 15, 1400–1419. <https://doi.org/10.1007/s11368-014-0881-9>.